Corrosion Science 77 (2013) 176–184

Contents lists available at ScienceDirect

Corrosion Science

journal homepage: www.elsevier.com/locate/corsci

Enhancement of corrosion protection of AISI 304 stainless steel by nanostructured sol–gel TiO_2 films

Lidija Ćurković [a,*], Helena Otmačić Ćurković [b], Sara Salopek [c], Marijana Majić Renjo [a], Suzana Šegota [d]

[a] Faculty of Mechanical Engineering and Naval Architecture, Ivana Lučića 5, Zagreb, Croatia
[b] Faculty of Chemical Engineering and Technology, Savska cesta 16, 10000 Zagreb, Croatia
[c] AC²T Research GmbH, Viktor Kaplan-Straße 2, 2700 Wiener Neustadt, Austria
[d] Ruđer Bošković Institute, Bijenička cesta 54, 10000 Zagreb, Croatia

ARTICLE INFO

Article history:
Received 11 May 2013
Accepted 29 July 2013
Available online 6 August 2013

Keywords:
A. Stainless steel
B. EIS
B. AFM
B. SEM
C. Oxide coatings

ABSTRACT

Nanostructured TiO_2 thin films were deposited on AISI 304 austenitic stainless steel by sol–gel process, dip coating technique. Influence of the number of layers, addition of polyethylene glycol (PEG) in initial sol, morphology and the surface roughness parameters of titania films on corrosion resistance of coated stainless steel were examined. Prepared films were characterized by SEM-EDS and AFM analysis. Electrochemical corrosion behavior of the coated stainless steel substrates was evaluated in simulated marine environment in 3 wt.% aqueous NaCl solution by electrochemical impedance spectroscopy (EIS) and in 0.5 M aqueous HCl solution by potentiodynamic polarization.

1. Introduction

One of the most common causes of metal components failure is damage due corrosion. Corrosion of metals cannot be totally eliminated, but its intensity can be reduced with the selection of appropriate materials for particular application, by using new alloys, corrosion inhibitors or protective films and coatings deposited onto the metal surface, especially in aggressive environments. Corrosion properties of stainless steels have been studied by a great number of authors. Stainless steels are known for their good corrosion resistance in many corrosive environments, but in the presence of chloride ions are susceptible to localized corrosion [1–4]. For that reason stainless steels are often additionally protected (coatings, corrosion inhibitors) when used in chloride environment. There is a current need for alternative coatings that can provide corrosion resistance to metal or alloy surfaces due to the environmental hazards posed by conventional coatings, such as chromates. Generally, ceramics and ceramic coatings with good passivity, low conductivity or insulating properties and good tribological properties show good corrosion resistance in aggressive media. Therefore, ceramics oxide films and coatings like TiO_2, Al_2O_3, ZrO_2, SiO_2, etc. can be deposited on metals to improve their surface properties [5–11]. There are several techniques for the deposition of ceramics films and coatings on metal substrate, such as chemical vapor deposition (CVD) [12], physical vapor deposition (PVD) [13], plasma spraying [14], electrochemical deposition [15] and sol–gel process [5,6,10,16–22]. The sol–gel method is an environmentally friendly technique of surface protection and had showed the potential for the replacement of toxic pretreatments and coatings which have traditionally been used for increasing corrosion resistance of metals. The sol–gel method, also known as chemical solution deposition, is a wet-chemical technique, a process involving following steps: hydrolysis and polycondensation, gelation, aging, drying, densification and crystallization. A sol–gel coating can be applied to a metal substrate through various techniques, such as dip-coating, spin-coating and spraying [16,22]. The most important advantages of sol–gel process are: low equipment costs, low processing temperature, good homogeneity, use of compounds that do not introduce impurities into the end product as initial substances thus making it "green", waste-free technology. These advantages make the sol–gel process one of the most appropriate technologies for preparation of thin, nanostructured films. Sol–gel technology has been significantly improved in the past 20 years.

Nanostructured coatings of titanium dioxide are interesting because of their good properties, such as high hardness, chemical stability and ability to provide effective protection to metal

* Corresponding author. Address: Faculty of Mechanical Engineering and Naval Architecture, Departmet of Materials, Ivana Lučića 5, 10000 Zagreb, Croatia. Tel.: +385 1 616 8313; fax: +385 1 615 7126.
E-mail address: lidija.curkovic@fsb.hr (L. Ćurković).

0010-938X/$ - see front matter © 2013 Elsevier Ltd. All rights reserved.
http://dx.doi.org/10.1016/j.corsci.2013.07.045

substrate, resistance to oxidation and wear, high refractive index, high dielectric constant, good antibacterial and photoelectrochemical properties [23,24].

In this paper, in order to improve corrosion behavior of stainless steel AISI 304 (X5CrNi18–10), ceramics nanostructured TiO_2 thin films were deposited on the steel surface by the sol–gel process, dip coating technique. Corrosion resistance of coated steel was examined in neutral and acid chloride media by means of electrochemical impedance spectroscopy (EIS) and polarization measurements. The influence of the titania films properties, such as number of layers, the surface roughness parameters and morphology on corrosion resistance of stainless steel was investigated.

2. Experimental procedure

2.1. Materials

For this study, austenitic stainless steel plates AISI 304 with dimensions of 10 × 10 × 2 mm were used as substrates. Chemical composition of the stainless steel was determined by the glow discharge optical emission spectroscopy (GDS 850A, Leco). Chemical composition of the investigated steel is shown in Table 1, and corresponds to stainless steel grade AISI 304 (X5CrNi18–10).

Before the deposition of films, steel substrates were ground with SiC abrasive discs (180–1000 grit) and then polished with diamond paste (3 μm and 0.25 μm). Substrates were then ultrasonically cleaned in acetone and subsequently dried prior to the deposition process.

2.2. Sol–gel TiO_2 films

For the preparation of colloidal solutions (TiO_2 sols), the following components were used:

(i) titanium (IV) isopropoxide ($Ti(C_3H_5O_{12})_4$)-TIP as a precursor,
(ii) *i*-propanol (C_3H_7OH)-POH as a solvent,
(iii) nitric acid (HNO_3) 0.5 M as a catalyst,
(iv) acetylacetone ($CH_3(CO)CH_2(CO)CH_3$)-AcAc as a chelating agent,
(v) polyethylene glycol, PEG ($H(OCH_2CH_2)_nOH$), *Mr* = 5000–7000, as an organic/polymer additive.

Two sols were prepared: sol 1 and sol 2. Sol 1 was prepared by dissolving titanium isopropoxide in i-propanol. A magnetic stirrer was used to continuously stir the liquid. Then, acetylacetone and nitric acid were added successively. Sol 1 was stirred vigorously for 2 h and after that it was sonicated for 30 min. Sol 2 was prepared using the same procedure as one described for sol 1 with only one exception, i.e. the addition of 2 g of polymer–polyethylene glycol (PEG).

The molar ratio of the reagents was: TIP:POH:AcAc:HNO_3 = 1:38.3:0.7:0.02, respectively.

Stainless steel plates were dipped once and three times into sol 1 and sol 2 by an in-house developed, electrically driven pulley system, simultaneously. Steel substrates were dipped into sol at a rate of 10 mm/min, then were held in solutions for 3 min, in order to allow surface wetting. The withdrawal speed was also 10 mm/min. After each dip, the steel substrates were dried at room temperature for 20 min. After drying at room temperature, each steel substrate was dried at 100 °C for an hour. After dip-coating and drying, each steel substrate was calcined at 550 °C for 4 h. After dipping, sol 1 and sol 2 were left at room temperature to allow the solvent to evaporate. After evaporation of the solvent, the gel was formed from sol 1 and sol 2 and calcined at 550 °C and prepared in the form of a powder. The powders were analyzed in terms of phase composition of TiO_2 by means of X-ray diffractometer (Philips PW3040/60 X'Pert PRO powder diffractometer, Almelo, The Netherlands) with Cu Kα radiation (λ = 1.54055 Å) at 45 kV and 40 mA.

2.3. Surface analysis

The morphology and chemical compositions of the TiO_2 films on steel substrates were determined by means of the scanning electron microscopy (Tescan Vega TS5136LS) equipped with the EDS detector.

The surface topography and the roughness of the TiO_2 films were determined by the Multimode AFM with a Nanoscope IIIa controller (Veeco Instruments Santa Barbara, CA) with a vertical engagement 125 μm scanner (JV). Contact mode imaging was performed under ambient conditions in air, by silicon tips (NP, Nom. Freq. 18 kHz, Nom. Spring constant of 0.06 N/m), and at a scan resolution of 512 samples per line. The linear scanning rate was optimized between 1.0 and 2.0 Hz at a scan angle of 0°. Images were processed and analyzed by means of the offline AFM NanoScope software, version 5.12r5. Roughness Analysis software option was used to perform roughness analyses on five different 2 μm × 2 μm imaged surface area for each sol–gel TiO_2 film. Results are presented as the R_a, R_q, R_z, R_{max} and the Z range values (mean ± standard deviation).

2.4. Electrochemical measurements

Measurements were performed by means of electrochemical methods (AC and DC techniques) at room temperature.

Electrochemical measurements were conducted in a conventional three electrode cell in simulated marine environment in near neutral 3 wt.% (0.51 M) aqueous NaCl solution as well as in 0.5 M HCl. All solutions were prepared from p.a. grade chemicals (Merck) and bidistilled water. Saturated calomel electrode (SCE) was used as a reference and platinum plate as the counter electrode. Measurements were performed using PAR 263A potentiostat/galvanostat and frequency response analyzer 1025.

Electrochemical impedance spectroscopy (EIS) measurements were conducted in 3 wt.% NaCl after 1 h immersion. Measurements were performed in the frequency range from 100 kHz to 0.01 Hz. The amplitude of the voltage perturbation was 0.01 V rms. All experiments were performed at open circuit potential.

Corrosion resistance of bare and coated stainless steel was also examined in 0.5 M HCl by means of polarization measurements. After 1 h of immersion in test solution, polarization curves were scanned in narrow (±0.02 V vs. open circuit potential) and wide (±0.15 V vs. open circuit potential) potential window. Potential scan rate was 0.166 mV s^{-1}. Data obtained in narrow potential window were used for the determination of the polarization resistance, i.e. linear polarization method, while the data obtained in wide potential window were analyzed by Tafel extrapolation method.

Table 1
The chemical composition of steel substrate, wt.%.

Elements	C	P	S	Si	Mn	Cu	Mo	Cr	Ni	Fe
wt.%	0.06	0.037	0.006	0.38	1.18	0.32	0.16	17.9	7.76	Balance

3. Results and discussion

3.1. SEM-EDX and XRD analysis

Fig. 1A and B shows surface morphology of TiO_2 film 1 and film 2 with three layers obtained by SEM analyses, while Fig. 1C and D represents their corresponding EDS spectra.

It is clear that the obtained films were free from cracks (Fig. 1A and B). Results of EDS spectra (Fig. 1C and D) of the coated surface of stainless steels confirm the uniform and compact TiO_2 film formation.

The crystalline structure of two calcined TiO_2 samples was analyzed by X-ray diffraction. The XRD patterns of both samples confirm the presence of two crystalline phases: anatase and rutile (Fig. 2A and B). By comparing the XRD patterns of both samples, it can be observed that powder 1 (TiO_2 powder without the addition of PEG) and powder 2 (TiO_2 powder with PEG) contain different amounts of anatase and rutile phase. Powder 2 has a higher amount of anatase phase and a lower amount of rutile phase than powder 1. During calcining, polyethylene glycol (PEG) degrades and slowes down the transformation from anatase phase to rutile phase, which explains why powder 2 contains a higher amount of anatase phase.

3.2. AFM analysis

Fig. 3 shows the three-dimensional AFM micrographs of the surface of one layer and three layers TiO_2 films, respectively. All images are presented as raw data except for the first-order two-dimensional flattening. Images were processed and analyzed by means of the offline AFM NanoScope software, version V5.31r1.

As shown in Fig. 3A–D the films reveal a surface morphology homogenously covered with titania layer with granular surface. For all deposited TiO_2 films following roughness parameters were determined: R_a (the arithmetic average of absolute values of the surface height deviations measured from the mean plane), R_q (the root mean square average of height deviations taken from the mean data plane), R_z (the average difference in height between five highest peaks and five lowest valleys relative to the mean plane), R_{max} (the maximum vertical difference in height between five highest peaks and five lowest valleys relative to the mean plane) and Z range (the maximum vertical distance between the highest and lowest data point within the analyzed region) values. The roughness parameters are obtained using Roughness analysis within Nanoscope V5.31r1 software. The roughness parameters of all investigated TiO_2 films are presented in Table 2.

All determined roughness parameters increase with the increasing number of layers (Table 2). The R_a values of the single-layer and three-layer sol–gel TiO_2 films without PEG are 2.10 ± 0.02 nm and 5.11 ± 0.04 nm, respectively. The R_a values were lower than those reported in the literature [25–27], indicating a possibility that the films are optically smooth [25]. The lower roughness value represents good homogeneity of the TiO_2 particles on the surface [28]. The surface morphology is also affected by the number of layers of TiO_2 film without the addition of PEG, which can be noted in the results of the roughness parameters presented in Table 2.

The addition of a small amount of PEG to a TiO_2 film changes the surface morphology, as well as the roughness parameters. With the addition of PEG, films become rougher. Roughness parameters (R_a, R_{max}, R_q, R_z and Z_{max}) are higher in comparison to the values found in a sol–gel TiO_2 film without the addition of PEG, which is in

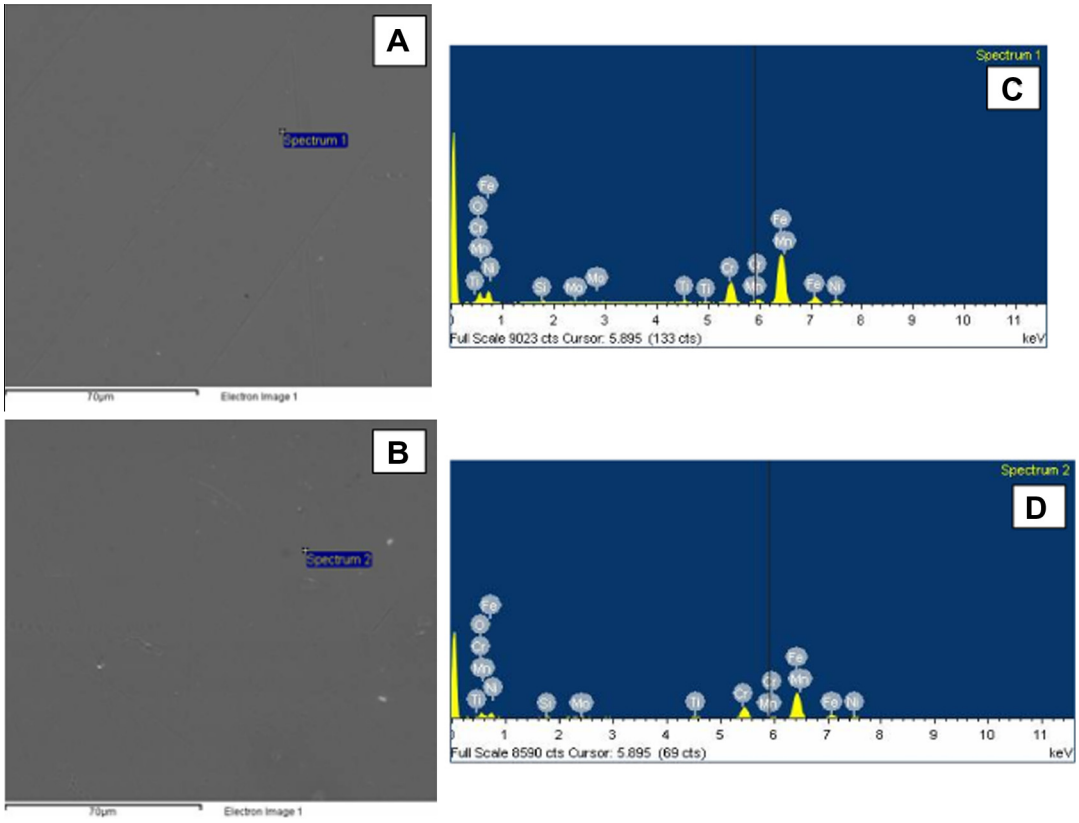

Fig. 1. SEM images of deposited sol–gel TiO_2 films on 304 type stainless steel: (A) TiO_2 film 1 with three layers; (B) SEM images of the surfaces of sol–gel TiO_2 film 2 with three layers; (C) EDS measurements of TiO_2 film 1 with three layers and (D) EDS measurements of TiO_2 film 2 with three layers. Film 1 (obtained from sol without PEG) and film 2 (obtained from sol with PEG).

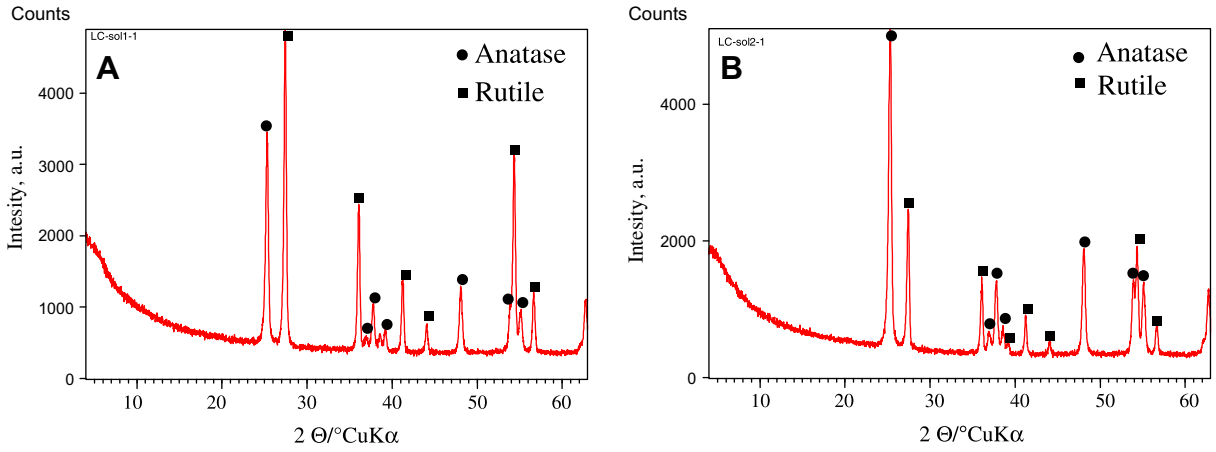

Fig. 2. XRD patterns of the TiO_2 powder prepared (A) without the addition of PEG to the initial sol 1 and (B) with the addition of PEG to the initial sol 2.

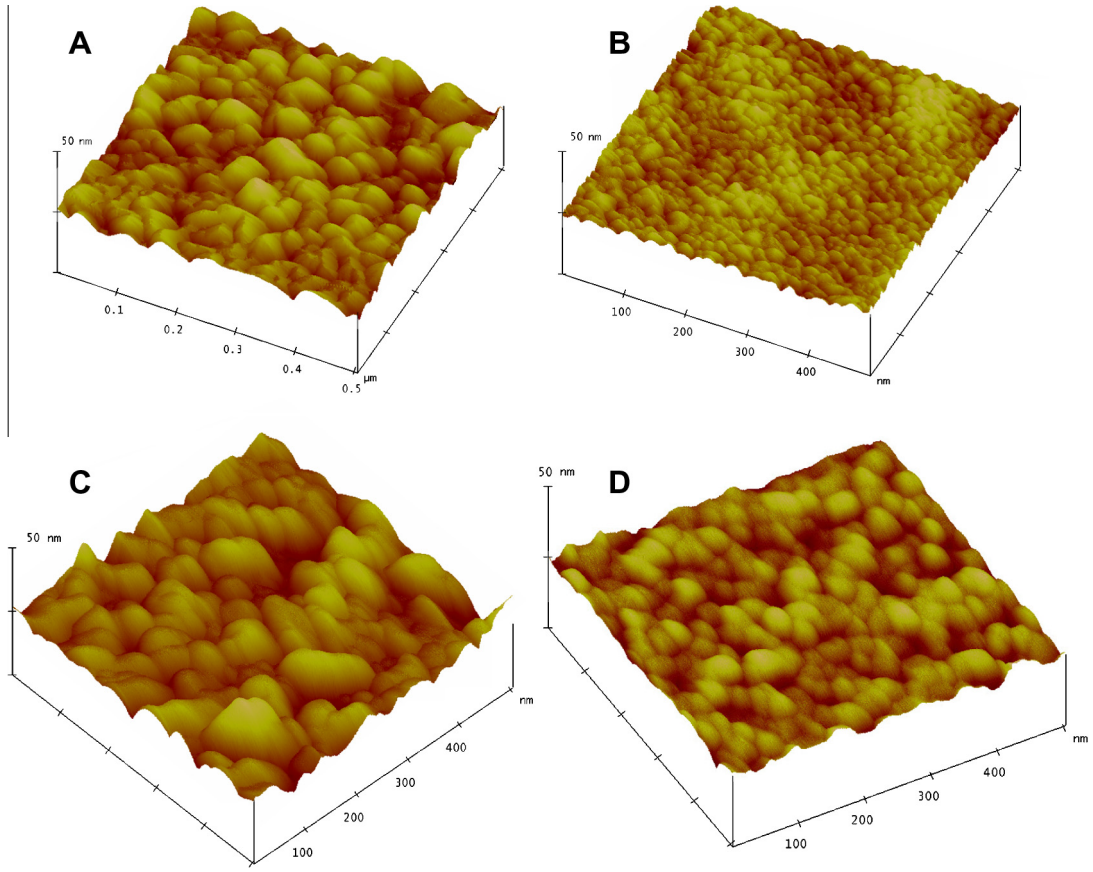

Fig. 3. Three dimensional AFM micrograph of deposited TiO_2 films: (A) TiO_2 film 1 with one layer, (B) TiO_2 film 1 with three layers, (C) TiO_2 film 2 with one layer and (D) TiO_2 film 2 with three layers. All images are taken in 500 nm × 500 nm area. Vertical scale in all images is 50 nm. Film 1 (obtained from sol without PEG) and film 2 (obtained from sol with PEG).

Table 2
The roughness parameters (mean value ± standard deviation – SD) of sol–gel TiO_2 film 1(obtained from sol without PEG) and film 2 (obtained from sol with PEG) with one layer and three layers.

Sol–gel TiO_2 film	R_a (nm), mean ± SD	R_q (nm), mean ± SD	R_z (nm), mean ± SD	R_{max} (nm), mean ± SD	Z_{max} (nm), mean ± SD
Film 1, one layer	2.10 ± 0.02	3.19 ± 0.04	3.98 ± 0.05	45.90 ± 0.6	46.7 ± 0.3
Film 1, three layers	2.69 ± 0.03	4.47 ± 0.06	4.88 ± 0.07	52.60 ± 0.3	56.8 ± 0.4
Film 2, one layer	5.11 ± 0.04	7.90 ± 0.06	12.60 ± 0.1	137.0 ± 0.8	137.0 ± 0.8
Film 2, three layers	10.20 ± 0.03	12.9 ± 0.05	38.6 ± 0.2	156.0 ± 0.9	159.0 ± 0.9

agreement with the results reported in literature [29]. Grain boundaries become less sharp and the matrix shows a smoother appearance. These results could be explained by assuming that the PEG adsorbed on the surface of TiO_2 particles produces stabilization by steric effects and leads to the formation of more compact and higher aggregates. Similar surface roughnesses was reported in [30,31].

Smoother surfaces favorably affect the chemical resistance of coatings, while increased surface roughness implies higher total surface, which can act to improve the photocatalytic activity [32]. The size (diameter) of titania particles present in films (Fig. 3) is found to in the range of 4–14 nm (Table 3) and particle height is found to be in the range of 1.1–2.1 (Table 3). These results reveal the formation of nanostructures on the surface of films.

3.3. Electrochemical impedance spectroscopy

Protective properties of TiO_2 films in 3 wt.% NaCl solution were examined by electrochemical impedance spectroscopy measurements. Corrosion potentials determined after 1 h of exposure to test solution are given in Table 4. Unprotected steel sample had the most negative corrosion potential, while the potentials of coated samples were more positive indicating decrease of anodic dissolution current. Actually, corrosion potential of TiO_2 coated samples is shifted into passive region of AISI 304 in NaCl solution [33].

Results obtained by EIS are presented in Fig. 4 (Nyquist plot) and Fig. 4 (Bode plot). As can be clearly seen from Fig. 4, impedances of all TiO_2 coated samples are significantly greater than those of the unprotected sample. For both kinds of TiO_2 films improvement of protective properties is observed with the increase of film thickness. Film 1, however, presents better protection than film 2.

EIS spectrum for bare AISI 304 (Fig. 5) exhibits one time constant, corresponding to corrosion process occurring at the metal surface. For TiO_2 coated samples at least two time constants can be observed (Fig. 5). The one in the high frequencies region (HF) can be attributed to the TiO_2 protective film. Time constant at lower frequencies (LF) is probably associated with the EIS response of the corrosion process occurring at the TiO_2/steel interface [34]. Appearance of LF time constant indicates that both kinds of TiO_2 films exhibit certain degree of porosity as corrosion process occurs on spots where electrolyte penetrates through the pores of the coating to the metal surface. The LF time constant is found at lower frequencies for film 1 than for film 2, for both one and three layers. Impedance spectra were fitted using the equivalent circuits given in Fig. 6. Fitted parameters are shown in Table 5, while solid lines in Figs. 4 and 5 represent the fitting curves. EIS spectra for bare stainless steel can be represented by simple equivalent circuit shown in Fig. 6 where R_{el} stands for the resistance of the electrolyte, R_{ct} charge transfer resistance of the steel, C_{dl} pseudocapacitance of double layer formed at the metal solution interface and n is a coefficient associated to the system homogeneity. Equivalent circuit describing the behavior of steel coated by film 2 (obtained from sol with PEG) is commonly proposed for metal covered by coating with defects [35]. In this circuit R_{pore} is the pore electrical resistance to the ionic current through the pores and C_{coat} represents the coating pseudocapacitance. In order to describe EIS spectra obtained for stainless steel protected by film 1 (obtained from sol without PEG) additional diffusion element was necessary at intermediate frequencies (Fig. 5C). This element, cotangent-hyperbolic diffusion impedance (O) represents the finite length diffusion inside the pores [36–38]. The impedance response for finite length diffusion is:

$$Z_D = \frac{\tanh[K_D(j\omega)^{0.5}]}{Y_0(j\omega)^{0.5}} \quad (1)$$

where $K_D = l/\sqrt{D}$ (2)

In this equation l represents pore length and D diffusion coefficient. Such equivalent electrical circuit was also used by Liu et al. [36,37] to describe behavior of steel covered by CrN PVD coating in 0.5 M NaCl and Lopez et al. [38] to describe behavior of multilayer silica-methacrylate hybrid coating on stainless steel.

The relatively low values of R_{pore} (Table 5) indicate that the electrolyte penetrates into the pores of coating. The highest R_{pore} value was obtained for the sample protected by film 1 with three layers indicating that this is the least porous coating. The fact that for interpretation of EIS data for film 1 additional diffusion element was necessary indicates that film 1 has denser and finer microstructure than film 2 coating for which corrosion process is not diffusion limited. K_D characterizes the time necessary for aggressive ions to diffuse through the pores, as expected, it is lower for coating with one layer than for the coating with two layers. The same applies for admittance related to the pore diffusion it is smaller for thicker coating. Polarization resistance of each sample can be determined as a sum of all resistive elements in the equivalent cir-

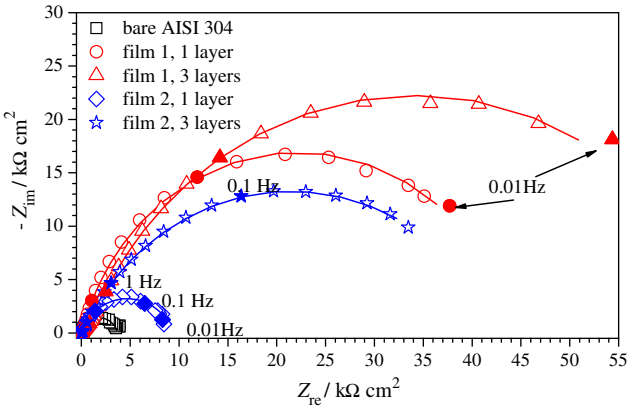

Fig. 4. Nyquist impedance plot for bare AISI 304 stainless steel and coated by two kinds of ceramic sol–gel TiO_2 films: film 1 (obtained from sol without PEG) and film 2 (obtained from sol with PEG) with one layer and three layers. Measurements were performed in 3 wt.% NaCl. Symbols represent experimental data and solid lines fitted data.

Table 3
Results of TiO_2 films particle height and diameter (mean value with corresponding standard deviation – SD) obtained from the analyzed area 500 nm × 500 nm.

Sol–gel TiO_2 film	Height (nm), mean ± SD	Diameter (nm), mean ± SD
Film 1, one-layer	1.8 ± 0.8	14 ± 20
Film 1, three-layer	2.1 ± 0.9	11 ± 12
Film 2, one-layer	1.6 ± 0.6	8 ± 16
Film 2, three-layer	1.1 ± 0.3	4 ± 11

Table 4
Corrosion potentials of bare AISI 304 stainless steel and coated with TiO_2 film 1 (obtained from sol without PEG) and film 2 (obtained from sol with PEG) in 3 wt.% NaCl solution.

Sample	Bare AISI 304	TiO_2 film1, one layer	TiO_2 film 1, three layers	TiO_2 film 2, one layer	TiO_2 film 2, three layers
E_{corr} (mV_{SCE})	−567	−306	−305	−478	−355

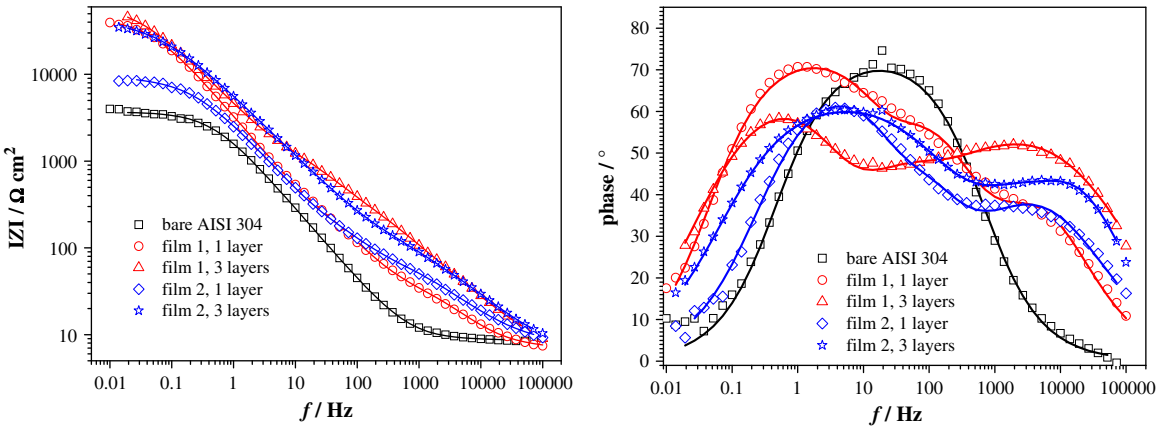

Fig. 5. Bode impedance plots for bare AISI 304 stainless steel and coated by two kinds of ceramic sol–gel TiO_2 films: film 1 (obtained from sol without PEG) and film 2 (obtained from sol with PEG) with one layer and three layers. Measurements were performed in 3 wt.% NaCl. Symbols represent experimental data and solid lines fitted data.

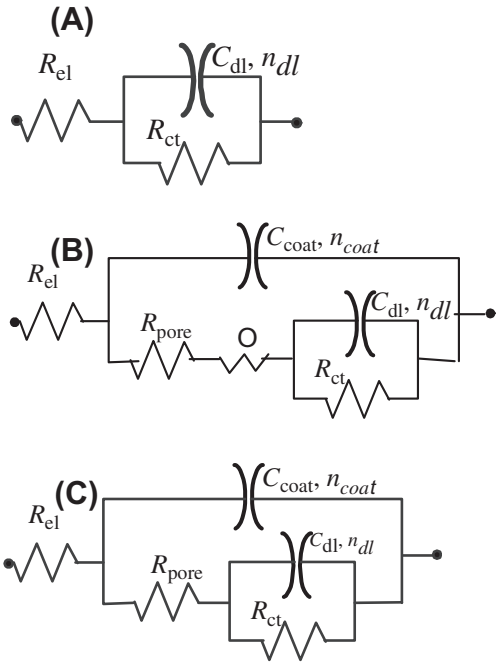

Fig. 6. Equivalent electrical circuits used to model impedance data: (A) bare AISI 304 stainless steel, (B) stainless steel protected by film 1 (obtained from sol without PEG) and (C) stainless steel protected by film 2 (obtained from sol with PEG).

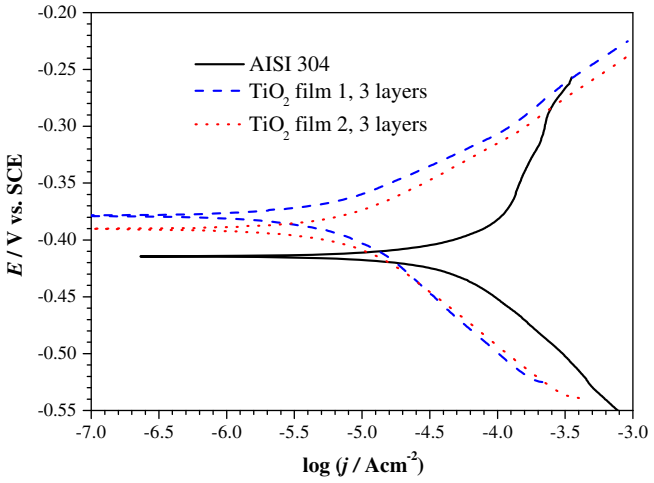

Fig. 7. Polarization curves obtained in 0.5 M HCl for stainless steel with and without sol–gel titania films with three layers: film 1 (obtained from sol without PEG) and film 2 (obtained from sol with PEG).

cuit (except the resistance of the electrolyte between working and reference electrode). It can be seen that the polarization resistance of AISI 304 stainless steel protected with only one layer of TiO_2 film 1 is twelve times greater than that of unprotected steel. When three layers of film 1 were applied, polarization resistance increased twenty times. For samples protected by film 2 similar behavior was observed, although the increase of polarization resistance was slightly lower. Improvement of polarization resistance obtained in this work is alike or even better than ones found in literature for various types of ceramic coatings. Ruhi et al. [21] examined the corrosion resistance of sol–gel alumina coatings on mild steel in 3.5% NaCl and the maximal increase of polarization resistance was about ten times. Cheragi et al. [39] studied corrosion behavior of TiO_2–NiO films on AISI 316L stainless steel in 3.5% NaCl. They have found that the highest degree of protection is obtained when four layers of ceramic coating are applied, in which case corrosion current decreased approximately six times.

Table 5
EIS fitting parameters for bare and coated AISI 304 stainless steel in 3 wt.% NaCl. Film 1 (obtained from sol without PEG) and film 2 (obtained from sol with PEG).

Sample	Bare AISI 304	TiO_2 film1, single layer	TiO_2 film 1, three layers	TiO_2 film 2, single layer	TiO_2 film 2, three layers
R_{pore} (Ω cm^2)	–	120	943	106	161
C_{coat} (μF cm^{-2})	–	1.97	1.33	2.97	1.31
n	–	0.87	0.66	0.69	0.69
Y_0 for O (μS s$^{1/2}$ cm^{-2})	–	338.2	112.5	–	–
K_D (s$^{1/2}$)	–	1.3	6.34	–	–
R_{ct} (kΩ cm^2)	3.37	32.2	68.1	9.03	42.5
C_{dl} (μF cm^{-2})	101	55.4	30.3	42.4	29.9
n_{dl}	0.83	0.91	1	0.81	0.79

Table 6
Corrosion parameters for bare and coated stainless steel in 0.5 M HCl determined by the Tafel extrapolation method. Film 1 (obtained from sol without PEG) and film 2 (obtained from sol with PEG).

Sample	E_{corr} (mV_{SCE})	j_{corr} ($\mu A\ cm^{-2}$)	b_a ($mV\ dec^{-1}$)	$-b_c$ ($mV\ dec^{-1}$)
Bare AISI 304	−414	64.85	91	128
TiO_2 film 1, three layers	−379	7.77	66	108
TiO_2 film 2, three layers	−390	10.01	77	101

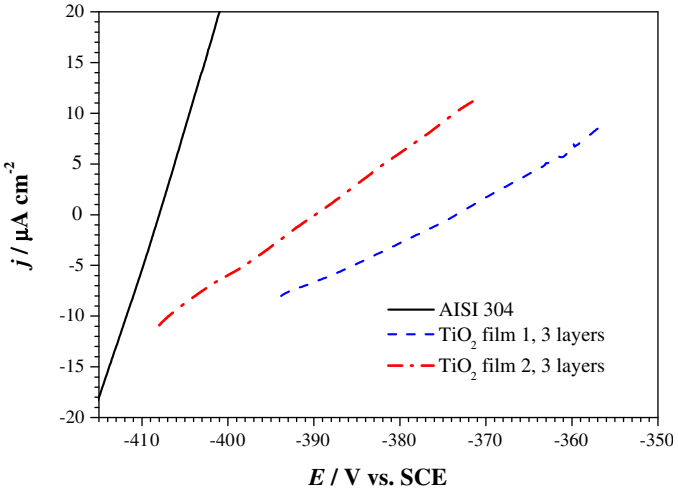

Fig. 8. Polarization curves obtained in narrow potential range for stainless steel with and without sol–gel titania films in 0.5 M HCl, film 1 (obtained from sol without PEG) and film 2 (obtained from sol with PEG).

3.4. Tafel extrapolation method

Behavior of bare and TiO_2 coated AISI 304 stainless steel in acidic chloride media was examined by means of polarization measurements in narrow and wide potential range. The acid chloride media is much more aggressive media than NaCl for that reason studies in acid media were performed only on samples protected by three-layer coatings. Polarization curves for bare stainless steel and three-layer TiO_2 films are given in Fig. 7. It can be seen that both films decrease corrosion rate of unprotected steel. Both anodic and cathodic current densities decreased for samples coated either by film1 or film 2 coating. Corrosion parameters: corrosion potential (E_{corr}), corrosion current density (j_{corr}) and anodic and cathodic Tafel slopes (b_a, b_c) were determined from polarization curves by Tafel extrapolation method (Table 6). The application of Tafel's law assumes that the interface is under kinetic control, in spite of the existence of aprotection layer. As the voltammetric curve indicates quite high currents, it is reasonable to assume that the systems are under active corrosion, therefore Tafel law applies.

Corrosion parameters presented in Table 6 confirm that titania film 1 exhibits better protection of underlying stainless steel than film 2. Unlike in neutral media, in acid corrosion potential of coated samples was not very much different from that of the bare sample.

Table 7
Corrosion parameters determined from linear polarization measurements in 0.5 M HCl. Film 1 (obtained from sol without PEG) and film 2 (obtained from sol with PEG).

Sample	j_{corr} ($\mu A\ cm^{-2}$)	R_p ($k\Omega\ cm^2$)
Bare AISI 304	20.52	1.115
TiO_2 film 1, three layers	8.31	2.140
TiO_2 film 2, three layers	11.65	1.628

3.5. Linear polarization

Studies of protective titania films in 0.5 M HCl were also performed by the polarization in the narrow potential range – linear polarization. Polarization curves obtained for AISI 304, bare and protected by three layers of examined titania films are given in Fig. 8.

The values of polarization resistance for each studied sample, determined from polarization curves (Fig. 8), are given in Table 7. Corrosion current densities were calculated according to Stern–Geary equation:

$$j_{corr} = \frac{B}{R_p} \tag{3}$$

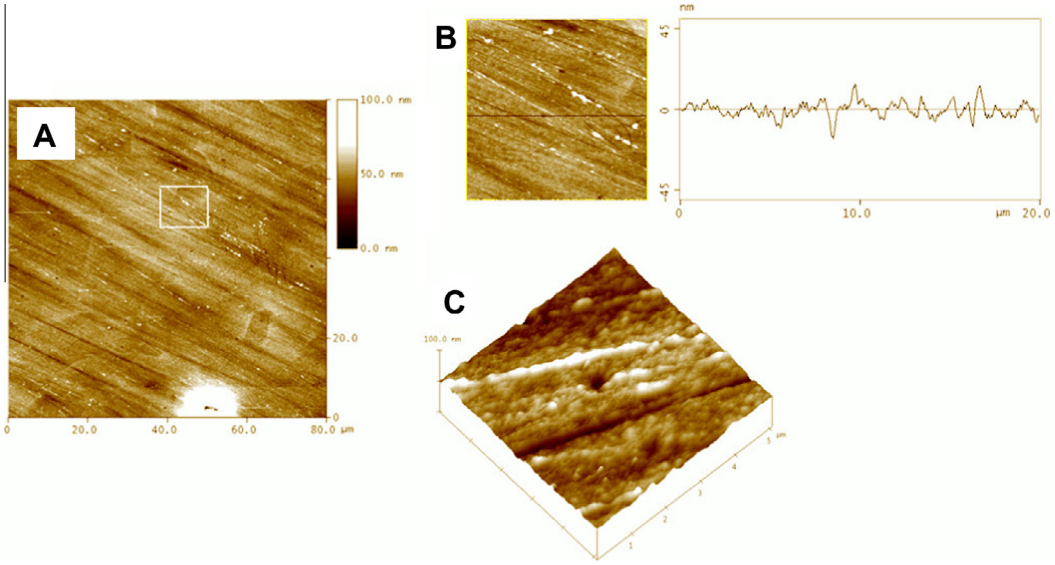

Fig. 9. AFM micrograph of sol–gel TiO_2 film 1 (obtained from sol without PEG) with three layers after corrosion. (A) Height image is taken in 80 μm × 80 μm area. Vertical scale is 80 nm. Surface topography is presented as a (B) zoomed height profile along the indicated lines ("Section analysis") of the denoted region on figure (A); (scan size 20 μm × 20 μm, vertical scale 90 nm); (C) a 3D-view of height data (scan size 5 μm × 5 μm, vertical scale 100 nm).

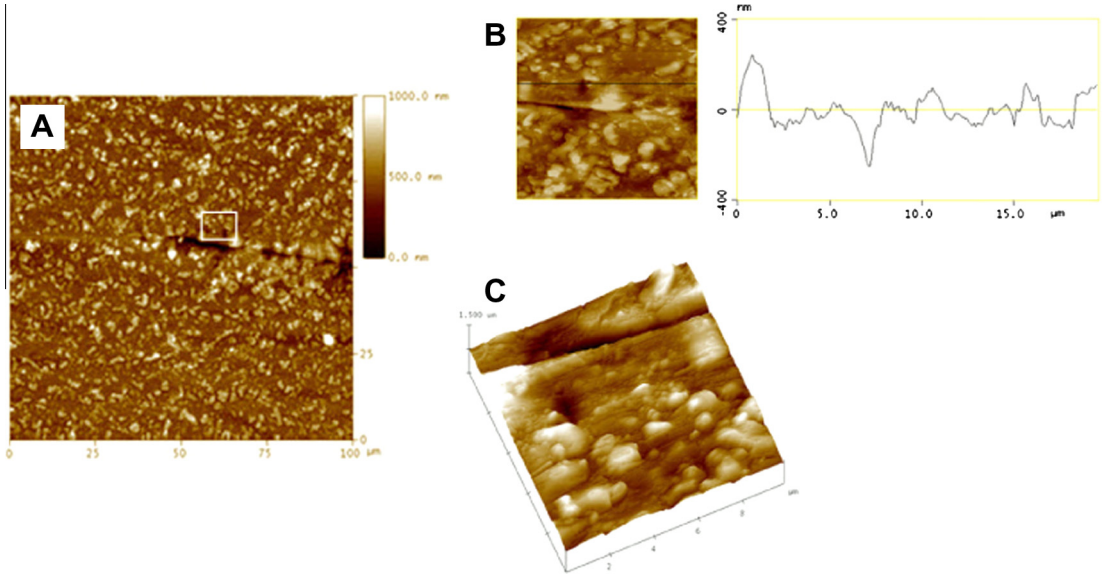

Fig. 10. AFM micrograph of sol–gel TiO_2 film 2 (obtained from sol with PEG) with three layers after corrosion. (A) Height image is taken in 100 μm × 100 μm area. Vertical scale is 1 μm. Surface topography is presented as a (B) zoomed height profile along the indicated lines ("Section analysis") of the denoted region on figure (A); (scan size 20 μm × 20 μm, vertical scale 800 nm); (C) a 3D-view of height data (scan size 5 μm × 5 μm, vertical scale 1500 nm).

where constant B is:

$$B = \frac{|b_a \cdot b_c|}{2.303 \cdot (b_a + |b_c|)} \quad (4)$$

Results obtained by linear polarization measurements confirm that in 0.5 M HCl coating of TiO_2 decreases the dissolution rate of underlying stainless steel. As in 3 wt.% NaCl better protection is achieved with titania film 1 than with film 2. However, in acid solution the polarization resistance of AISI 304 coated by three layers of TiO_2 film 1 is only nine times bigger than that of unprotected sample while in neutral media this ratio was 20:1. HCl is more aggressive medium than NaCl and the corrosion process that may occur in pores is much faster (R_p of stainless steel in acid is ten times lower than in neutral chloride media), which may lead to accumulation of corrosion products at the TiO_2/metal interface, promoting the formation of defects and micro-cracks in the coating.

3.6. AFM analysis after exposure to 0.5 M HCl

The morphology of film 1 and film 2 with three layers after exposure to 0.5 M HCl (after polarization studies) is analyzed by AFM. The AFM imaging of both films reveals the corrosion effect on the investigated surfaces (Figs. 9 and 10). While the structure of the film 1 after corrosion remained grainy with randomly placed pores with its depth of 40 nm, the film 2 surface displays significant effect of corrosion. There is appearance of pores whose depth reaches values up to 500 nm.

Yu et al. [40] has examined the influence of PEG addition on the photocatalytic activity of TiO_2 films prepared by the sol–gel method. They came to the conclusion that surface structure and photocatalytic activity of resultant thin films formed on soda-lime plate substrates significantly depends on the concentration of PEG in the precursor solution. Their work indicates that during the heat treatment, decomposition of PEG occurs, which results in the formation of pores in the TiO_2 film. The diameters of such pores were found to be 100–500 nm depending on PEG concentration.

In our work it was observed that PEG contributes to higher surface roughness of titania films, but it is also quite possible that fine pores have formed during the heat treatment of the film due to the PEG decomposition. Through these pores electrolyte may penetrate and reach steel surface leading to its corrosion. AFM examination of both coatings after exposure to 0.5 M HCl (Fig. 10) clearly shows that deeper and larger pores develop on film 2 than on film 1. This explains the results obtained by EIS that have indicated much easier diffusion of aggressive species through film 2 than film 1 coating. This is also the reason why film 1 exhibits better protective properties than film 2.

4. Conclusions

1. Titania films, free from cracks uniform and compact, were coated on 304 stainless steel by sol–gel method with and without addition PEG in initial sol.
2. AFM measurements of the titania coated stainless steel specimens confirms the nanostructured nature of the films.
3. After exposure to corrosive media, it was found that the surface of both films exhibits small pores, especially for the film prepared with addition of PEG.
4. EIS measurements have proven that corrosion resistance of stainless steel in a simulated marine environment in 3 wt.% of NaCl solution, increases with increasing the number of layers of both sol–gel TiO_2 films. The highest polarization resistance was obtained for steel protected by sol–gel TiO_2 film with three layers prepared without addition of PEG.
5. Corrosion parameters determined by Tafel polarization and linear polarization method in 0.5 M HCl showed that deposited sol–gel TiO_2 all films significantly improved the corrosion resistance of investigated stainless steel. The best corrosion protection results were obtained by sol–gel TiO_2 film obtained from the sol without addition of organic additive PEG.

Acknowledgement

This study was supported by the Ministry of Science, Education and Sports of the Republic of Croatia within the framework of the Projects Nos. 120-1201833-1789, 125-1252973-2572 and 098-0982934-2744.

References

[1] Q. Hu, G. Zhang, Y. Qiu, X. Guo, The crevice corrosion behaviour of stainless steel in sodium chloride solution, Corros. Sci. 53 (2011) 4065–4072.
[2] Z. Wang, Y. Cong, T. Zhang, Y. Shao, G. Meng, Study on the crevice corrosion behavior of 316L stainless steel used on marine gas turbine inlet filters by stochastic methods, Int. J. Electrochem. Sci. 6 (2011) 5521–5538.
[3] Y. Yin, L. Niu, M. Lua, W. Guo, S. Chen, In situ characterization of localized corrosion of stainless steel by scanning electrochemical microscope, Appl. Surface Sci. 255 (2009) 9193–9199.
[4] Y. Wang, W. Wang, Y. Liu, L. Zhong, J. Wang, Study of localized corrosion of 304 stainless steel under chloride solution droplets using the wire beam electrode, Corros. Sci. 53 (2011) 2963–2968.
[5] G.X. Shen, J.C. Chen, C.J. Lin, Corrosion protection of 316L stainless steel by a TiO_2 nanoparticle coating prepared by sol–gel method, Thin Solid Films 489 (2005) 130–136.
[6] G. Ruhi, O.P. Modi, I.B. Singh, Pitting of AISI 304L stainless steel coated with nano structured sol–gel alumina coatings in chloride containing acidic environments, Corros. Sci. 51 (2009) 3057–3063.
[7] C.X. Shan, X. Hou, K.-L. Choy, Corrosion resistance of TiO_2 films grown on stainless steel by atomic layer deposition, Surf. Coat. Technol. 202 (2008) 2399–2402.
[8] Z.F. Zhou, E. Chalkova, S.N. Lvov, P. Chou, R. Pathania, Development of a hydrothermal deposition process for applying zirconia coatings on BWR materials for IGSCC mitigation, Corros. Sci. 49 (2007) 830–843.
[9] N. Padhy, U. KamachiMudali, V. Chawla, R. Chandra, B. Raj, Corrosion behaviour of single (Ti) and duplex (Ti–TiO_2) coating on 304L stainless steel in nitric acid medium, Mater. Chem. Phys. 130 (2011) 962–972.
[10] J. Gallardo, A. Duran, J.J. de Damborenea, Electrochemical and in vitro behaviour of sol–gel coated 316L stainless steel, Corros. Sci. 46 (2004) 795–806.
[11] V.S. Saji, J. Thomas, Nanomaterials for corrosion control, Curr. Sci. 92 (2007) 51–55.
[12] R. Hausbrand, B. Bolado-Escudero, A. Dhont, J. Wielant, Corrosion of flame-assisted CVD silica-coated steel sheet, Corros. Sci. 61 (2012) 28–34.
[13] A. Perez, A. Billard, C. Rébéré, C. Berziou, S. Touzain, J. Creus, Influence of metallurgical states on the corrosion behaviour of Al–Zn PVD coatings in saline solution, Corros. Sci. 74 (2013) 240–249.
[14] Y. Wang, W. Tiana, T. Zhang, Y. Yang, Microstructure, spallation and corrosion of plasma sprayed Al_2O_3–13%TiO_2 coatings, Corros. Sci. 51 (2009) 2924–2931.
[15] E. Setare, K. Raeissi, M.A. Golozar, M.H. Fathi, The structure and corrosion barrier performance of nanocrystalline ZrO_2 electrodeposited coating, Corros. Sci. 51 (2009) 1802–1808.
[16] S.K. Tiwari, M. Tripathi, R. Singh, Electrochemical behavior of zirconia based coatings on mild steel prepared by sol–gel method, Corros. Sci. 63 (2012) 334–341.
[17] S. Šegota, L. Ćurković, D. Ljubas, V. Svetličić, I. Fiamengo-Houra, N. Tomašić, Synthesis, characterization and photocatalytic properties of sol–gel TiO_2 films, Ceram. Int. 37 (2011) 1153–1160.
[18] M. Atik, P.L. Neto, L.A. Avaca, M.A. Aegerter, Sol–gel thin films for corrosion protection, Ceram. Int. 21 (1995) 403–406.
[19] R. Gheriani, R. Chtourou, Preparation of nanocrystalline titanium dioxide (TiO_2) thin films by the sol–gel dip coating method, J. Nano Res. 16 (2012) 105–111.
[20] S. Li, J. Fu, Improvement in corrosion protection properties of TiO_2 coatings by chromium doping, Corros. Sci. 68 (2013) 101–110.
[21] G. Ruhi, O.P. Modi, A.S.K. Sinha, I.B. Singh, Effect of sintering temperatures on corrosion and wear properties of sol–gel alumina coatings on surface pre-treated mild steel, Corros. Sci. 50 (2008) 639–649.
[22] T.L. Metroke, R.L. Parhhill, E.T. Knobbe, Passivation of metal alloys using sol–gel-derived materials-review, Prog. Org. Coat. 41 (2001) 233–238.
[23] E. Alkhateeb, R. Ali, S. Virtanen, N. Popovska, Electrochemical evaluation of the corrosion behavior of steel coated with titanium-based ceramic layers, Surface Coat. Technol. 205 (2011) 3006–3011.
[24] X. Chen, S.S. Mao, Titanium dioxide nanomaterials: synthesis, properties, modifications, and applications, Chem. Rev. 107 (2007) 2891–2959.
[25] M.A. Hamid, I. Ab, Rahman, preparation of titanium dioxide (TiO_2) thin films by sol gel dip coating method, Malaysian J. Chem. 5 (2003) 086–091.
[26] K. Jungsuwattananon, S. Saesoo, N. Pimpha, N. Negishi, Characterization and bactericidal activity of thin-film TiO_2 photocatalyst, CMU J. Nat. Sci. Spec. Issue Nanotechnol. 7 (2008) 25–31.
[27] M. Bernardi, E.J.H. Lee, P.N. Lisboa-Filho, E.R. Leite, E. Longo, J.A. Varela, TiO_2 thin film growth using the MOCVD method, Mater. Res. 4 (2001) 223–226.
[28] P. Alphonse, R. Bleta, R. Soules, Effect of PEG on rheology and stability of nanocrystallinetitania hydrosols, J. Colloid Interface Sci. 337 (2009) 81–87.
[29] J.C. Yu, W. Ho, J. Yu, S.K. Hark, K. Iu, Effects of trifluoroacetic acid modification on the surface microstructures and photocatalytic activity of mesoporous TiO_2 thin films, Langmuir 19 (2003) 3889–3896.
[30] J.M. Valtierra, M. Sanchez-Cardenas, C. Frausto-reyes, S. Calixto, Formation of smooth and rough TiO_2 thin films on fiberglass by sol–gel method, J. Mex. Chem. Soc. 50 (2006) 8–13.
[31] I.K. Konstantinou, T.A. Albanis, TiO_2-assisted photocatalytic degradation of azo dyes in aqueous solution: kinetic and mechanistic investigations: a review, Appl. Catal. B: Environ. 49 (2004) 1–14.
[32] D. Wang, G.P. Bierwagen, Sol–gel coatings on metals for corrosion protection, Prog. Org. Coat. 64 (2009) 327–338.
[33] R.Z. Zand, K.. Verbeken, A. Adriaens, Corrosion resistance performance of cerium doped silica sol–gel coatings on 304 L stainless steel, Prog. Org. Coat. 75 (2012) 463–473.
[34] R.A. Antunes, M.C.L. de Oliveira, M.F. Pillis, Effect of the deposition temperature on the corrosion stability of TiO_2 films prepared by metal organic chemical vapor deposition, Int. J. Electrochem. Sci. 8 (2013) 1487–1500.
[35] F. Mansfeld, M.W. Kenedig, S. Tsai, Evaluation of corrosion behavior of coated metals with AC impedance measurements, Corrosion 38 (1982) 478–485.
[36] C. Liu, Q. Bi, A. Leyland, A. Matthews, An electrochemical impedance spectroscopy study of corrosion behaviour of PVD coated steels in 0.5 N NaCl aqueous solution: Part I. Establishment of equivalent circuits for EIS data modeling, Corros. Sci. 45 (2003) 1243–1256.
[37] C. Liu, Q. Bi, A. Leyland, A. Matthews, An electrochemical impedance spectroscopy study of corrosion behaviour of PVD coated steels in 0.5 N NaCl aqueous solution: Part II. EIS interpretation of corrosion behaviour, Corros. Sci. 45 (2003) 1257–1273.
[38] D.A. Lopez, N.C. Rosero-Navarro, J. Ballarre, A. Duran, M. Aparicio, S. Cere, Multilayer silica-methacrylate hybrid coatings prepared by sol–gel on stainless steel 316 L: electrochemical evaluation, Surf. Coat. Technol. 202 (2008) 2194–2201.
[39] H. Cheraghi, M. Shahmiri, Z. Sadeghian, Corrosion behavior of TiO_2–NiO nanocomposite thin films on AISI 316L stainless steel prepared by sol–gel method, Thin Solid Films 522 (2012) 289–296.
[40] J. Yu, X. Zhao, Q. Zhao, Effect of surface structure on photocatalytic activity of TiO_2 thin films prepared by sol–gel method, Thin Solid Films 379 (2000) 7–14.